

Constraining Multi-scale Pairwise Features between Encoder and Decoder Using Contrastive Learning for Unpaired Image-to-Image Translation

Xiuding Cai,^{1,2} Yaoyao Zhu,^{1,2} Dong Miao^{1,2} Linjie Fu^{1,2} Yu Yao^{1,2*}

¹ Chengdu Institute of Computer Application, Chinese Academy of Sciences, Chengdu

² University of Chinese Academic Science, Beijing, China

{caixiuding20, zhuyaoyao19, miaodong20, fulinjie19}@mails.ucas.ac.cn, yaoyu@casit.com.cn

Abstract

Contrastive learning (CL) has shown great potential in image-to-image translation (I2I). Current CL-based I2I methods usually re-exploit the encoder of the generator to maximize the mutual information between the input and generated images, which does not exert an active effect on the decoder part. In addition, though negative samples play a crucial role in CL, most existing methods adopt a random sampling strategy, which may be less effective. In this paper, we rethink the CL paradigm in the unpaired I2I tasks from two perspectives and propose a new one-sided image translation framework called EnCo. First, we present an explicit constraint on the multi-scale pairwise features between the encoder and decoder of the generator to guarantee the semantic consistency of the input and generated images. Second, we propose a discriminative attention-guided negative sampling strategy to replace the random negative sampling, which significantly improves the performance of the generative model with an almost negligible computational overhead. Compared with existing methods, EnCo acts more effective and efficient. Extensive experiments on several popular I2I datasets demonstrate the effectiveness and advantages of our proposed approach, and we achieve several state-of-the-art compared to previous methods.

Introduction

Image-to-image translation (I2I) aims to convert images from one domain to another with content preserved as much as possible. I2I tasks have received a lot of attention given their wide range of applications, such as style transfer (Ulyanov, Vedaldi, and Lempitsky 2016), semantic segmentation (Yu, Koltun, and Funkhouser 2017; Kirillov et al. 2020), super resolution (Yuan et al. 2018), colorization (Zhang, Isola, and Efros 2016), dehazing (Dong et al. 2020) and image restoration (Liang et al. 2021) etc.

In the absence of sufficient content constraints between the input and the generated images, applying adversarial loss (Goodfellow et al. 2014) in unpaired I2I tasks is often prone to model collapse. To this end, CycleGAN (Zhu et al. 2017), DiscoGAN (Kim et al. 2017), and DualGAN (Yi et al. 2017) propose cycle consistency, that assumes the generated

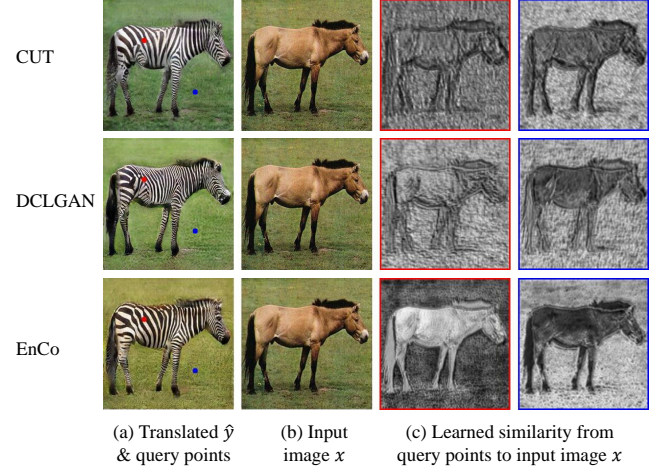


Figure 1: **Visualization of the learned features similarity between the encoder and decoder of the generator.** Given two query points sampled from the foreground (red) and background (blue) in (a), we compute $\exp(q \cdot k/\tau)$ with (b) to obtain their similarity map as shown in (c), respectively. Compared with the similarity learned by CUT and DCLGAN, similarity maps of EnCo are more compact, which demonstrates that our method learns distinguishing representation in a fine-grained level.

images should be able to be reconverted to the original images in some way. However, this assumption requiring bijection between the source domain and the target domain appears too strict (Park et al. 2020). For instance, the city street view is converted into a certain pixel-level annotated label, but reconvert a label to a city street view has yet countless possibilities. Such ill-posed settings limit the performance of cycle-consistency-based GANs, thus leading to blurred generations (Chen et al. 2020a). In addition, the performance of cycle consistency is stunted on some tasks involving large geometric changes (e.g., *Cat*↔*Dog*) (Park et al. 2020).

Recently, contrastive learning (CL) has achieved great success in the field of unsupervised representation learning (Hjelm et al. 2018; Chen et al. 2020b; He et al. 2020; Henaff 2020; Oord, Li, and Vinyals 2018). CL aims to learn an embedding space in which the relevant signals are brought together while the irrelevant signals are pushed

*Corresponding author.

Copyright © 2022, Association for the Advancement of Artificial Intelligence (www.aaai.org). All rights reserved.

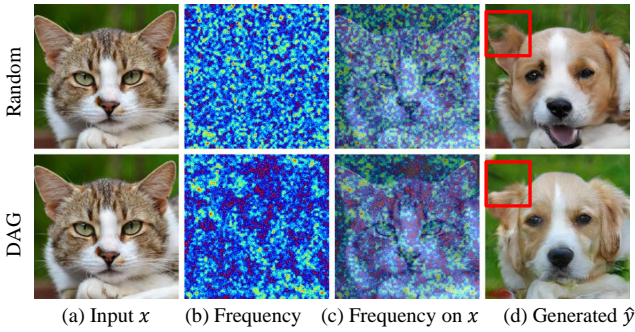


Figure 2: Comparison of different negative sampling strategy. For the input image x , we superimpose the negative sampling positions every 10 epochs to obtain the sampling frequency map (b). As can be seen from (c), compared to the random negative sampling strategy, our proposed DAG negative sampling strategy are more focused on regions that help in domain discrimination, such as ears, eyes, nose, etc. As can be seen in the red box in (d), the random negative sampling strategy, in the generated ear region, shows obvious artifacts, while DAG negative sampling strategy generates successful results.

apart. CUT (Park et al. 2020) is the first model to introduce CL to unpaired I2I tasks and demonstrates superior performance over cycle consistency-based frameworks.

To map the images to the embedding space, CUT exploits the encoder in the generator followed by a two-layer projection MLP. However, using one encoder and projection MLP to encode both input and generated images *may not efficiently capture the domain gap between the two domains*. For this, DCLGAN (Han et al. 2021) extends CUT to a dual way setting, enabling exploiting two separate encoders and projection MLPs for the encoding of the input and generated images, respectively. However, DCLGAN doubles the network parameters and computation effort of CUT, and sometimes, the bidirectional conversion is not desirable.

It is also important to note that the CL-based image translation methods, typified by CUT, do not have an explicit optimization effect on the decoder as they only reuse the encoder part in the generator. In this paper, we rethink the CL paradigm applied to I2I tasks by explicitly constraining the semantic consistency of multi-scale pairwise features between the **E**ncoder and **D**e**C**oder of the generator using CL (EnCo), thus guaranteeing content similarity between the input and generated images during one forward propagation. As shown in Figure 1, thanks to the explicit optimization on the decoder, EnCo learns a fine-grained semantic similarity between the encoder and decoder of the generator. Our method combines the advantages of CUT and DCLGAN and achieves better image generation performance than DCLGAN while requiring only even lower computational resources than CUT.

In addition, both CUT and DCL adopt a random negative sampling strategy, which may not be efficient enough (Wang et al. 2021). A well-defined negative sampling strategy can accelerate the convergence of the model and increase the learning curve so as to learn better feature representa-

tions (Cai et al. 2020). Recently, some approaches (Wang et al. 2021; Zheng, Cham, and Cai 2021; Lin et al. 2022) have explored the application of negative sampling strategy in CL-based approaches in I2I tasks and yielded improved performance. However, these methods usually require higher computational complexity. Meanwhile, they ignore the potential role of the discriminator in the process of negative sampling, which provides the truthfulness of the generated images. We design a discriminative attention-guided (DAG) negative sampling strategy that takes full advantage of the discriminative information provided by the discriminator to select more discriminative negative samples for optimization. Experiments show that our negative sampling strategy significantly boost the performance of generative model with almost negligible computational overhead. Figure 2 gives an example of how DAG negative sampling strategy affects the generating results. Our contributions are as follows.

- We propose EnCo, an efficient one-sided image translation framework based on CL. EnCo explicitly constrains the semantic consistency of multi-scale pairwise features between the encoder and decoder, thus to guarantee content similarity between the input and generated images.
- We rethink the potential role of discriminators in negative sampling and propose the DAG negative sampling strategy. This strategy improves network performance significantly while only requiring an almost negligible amount of computation.
- Extensive experiments on several popular I2I benchmarks reveal the effectiveness and advantages of our proposed method. We achieve several state-of-the-art compared to previous methods.

Related Works

Image-to-Image Translation

Image-to-image translation (Isola et al. 2017; Wang et al. 2018b; Zhu et al. 2017; Park et al. 2020; Wang et al. 2021) aims to transform images from the source domain to the target domain with the semantic content preserved. Pix2Pix (Isola et al. 2017) was the first framework to accomplish the I2I task using paired data with an adversarial loss (Goodfellow et al. 2014) and a reconstruction loss. However, paired data across domains are infeasible to be collected in most settings. Methods such as CycleGAN (Zhu et al. 2017), DiscoGAN (Kim et al. 2017) and DualGAN (Yi et al. 2017) extend the I2I task to an unsupervised setting based on cycle consistency assumption that the generated image should be able to be converted back to the original image again. In addition, UNIT (Liu, Breuel, and Kautz 2017) and MUNIT (Huang et al. 2018) propose to learn a shared hidden space for the source and target domain images, and then reconstruct the original image and generate the target domain image from the hidden space by applying two decoders.

Break the cycle

Cycle consistency (Zhu et al. 2017) requires underlying bijection between two distinct domains, which is sometimes

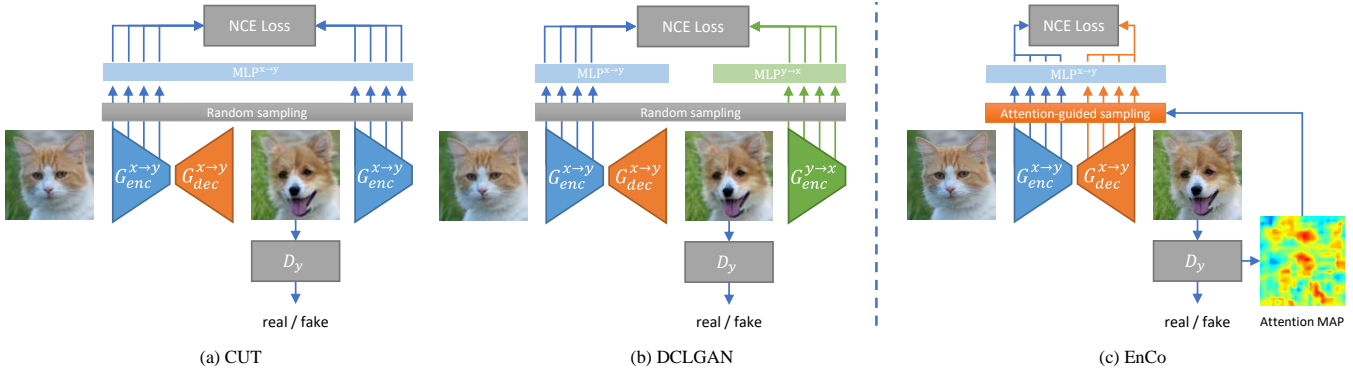


Figure 3: **A comparison of different CL-based image translation frameworks.** CUT reuses the encoder of the generator $G_{enc}^{\mathcal{X} \rightarrow \mathcal{Y}}$ as the encoder of both the input and generated images, and uses a network weight sharing two-layer projection MLP. DCLGAN adds an opposite conversion direction from the target domain to the source domain (the direction not drawn), using the encoders of the generators of the two conversion directions, $G_{enc}^{\mathcal{X} \rightarrow \mathcal{Y}}$ and $G_{enc}^{\mathcal{Y} \rightarrow \mathcal{X}}$, as the encoders of the input and generated images, respectively, and using two separate two-layer projection MLPs. our approach can be viewed as an implicit encoding CUT-like approach that directly constrains the semantic consistency of the multi-scale features of the encoder and decoder of the generator. In addition, we use a discriminative attention-guided negative sampling strategy compared to the random negative sampling strategy used by CUT and DCLGAN.

too strict and thus limits the performance of the generative networks. Some methods (Shrivastava et al. 2017; Fu et al. 2019) achieve one-sided translation by designing special distance functions to bypass cycle consistency. These require, for example, that the distances between input images and output images should be consistent (Benaim and Wolf 2017). Since the per-pixel reconstruction loss does not reflect human perceptual preferences well, some recent studies have attempted to re-purposed the pre-trained VGGNet (Simonyan and Zisserman 2015) as a perceptual loss to require that the input and output images should be visually consistent (Zheng, Cham, and Cai 2021). There may be a priori limitations in these methods, such as the frozen network weights of the loss function cannot adapt to the data and thus may not be the most appropriate (Zheng, Cham, and Cai 2021). For this reason, CUT (Park et al. 2020) proposes multi-layer PatchNCE Loss to maximize the mutual information between patches of input and output images based on CL. DCL (Han et al. 2021) extends CUT to a dual-way settings that exploiting two independent encoders and projectors for input and generated images respectively, but doubles the number of network parameters. Our work combines the advantages of CUT and DCL, allowing for better implicit encoding while keeping the network parameters the same as CUT or even less.

Contrastive Learning

Recently, contrastive learning has achieved impressive results in the field of unsupervised representation learning (Hjelm et al. 2018; Chen et al. 2020b; He et al. 2020; Henaff 2020; Oord, Li, and Vinyals 2018). Based on the idea of discriminative, CL aims to bring closer the representation of two correlated signals in the embedding space while pushing away the representation of uncorrelated signals. The design of the positive and negative is task-specific. For example, in image classification, positive samples can be images

with two different data augmentations and negative samples be any two different images (Chen et al. 2020b); in video-related tasks, positive samples can be any two clips from the same video and negative samples be clips from different videos (Qian et al. 2021). Based on the property of dense prediction in the I2I task, the associated signals of I2I can be naturally designed as pixel or patch corresponding between the original image and the generated image. CUT (Park et al. 2020) is the first method to maximize the mutual information between the input and generated images using the noisy contrastive estimation framework for the I2I task.

Negative Sampling

The selection of negative samples is crucial for CL (Robinson et al. 2020). The negative sampling methods can be generally classified into the following three categories (Park et al. 2020): a) static negative sampling (Chopra, Hadsell, and LeCun 2005), namely random negative sampling, which is the most commonly used negative sampling strategy for CL with no added prior. This type of method suffers from long convergence time and the curse of small batch size. b) dynamic negative sampling (Zhang et al. 2013; Rao, He, and Lin 2016; Ying et al. 2018). negatives are sampled by scoring anchor, positive, negative through a scoring function that obeys the probability function of the score. c) adversarial negative sampling (Wang et al. 2018a; Hu et al. 2021). This type of method generates hard negatives by adversarial generation, rather than selecting negatives by sampling.

Negative Sampling in Image-to-Image Translation

CUT and DCL both adopt the strategy of random negative sampling. Recently, some approaches (Hu et al. 2022; Wang et al. 2021; Lin et al. 2022) committed to improving the random sampling strategy in CL-based image translation. QS-Attn dynamically selects relevant anchor points as positive and negatives by computing the QKV matrix. NEG-

CUT (Wang et al. 2021) generates hard negatives by adversarial generation, thus replacing the sampling of negatives. PUT (Lin et al. 2022) proposes a negatives pruning strategy that uses fewer and better negative samples to achieve better generative performance. However, these methods require high computation cost. Our work reuses outputs from the discriminator to create an attention scoring map to guide the sampling of negatives, which is lightweight with almost negligible computation overhead, while it boost model performance significantly.

Methods

In this paper, we propose EnCo, an efficient one-sided image translation framework using CL. Differentiate from previous CL-based approaches, as shown in Figure 3, we explicitly constrain the semantic consistency of multi-scale pairwise features between the encoder and decoder of generator, instead of re-encoding the input image and the generated image to map them to the embedding space. In addition, we design a DAG negative sampling strategy to sample more discriminative negatives with attention for optimization.

Explicitly Constraining the Semantic Consistency of Multi-scale Pairwise Features between the Encoder and Decoder of the Generator

Given an image from the source domain $x \in \mathcal{X}$, our goal is to learn a mapping function (also called a generator) $G_{\mathcal{X} \rightarrow \mathcal{Y}}$ that converts the image from the source domain to the target domain \mathcal{Y} , i.e., $\hat{y} = G_{\mathcal{X} \rightarrow \mathcal{Y}}(x)$, and with as much content semantic information preserved as possible.

An intuition is that we can maintain the semantic consistency among the features generated by the sequence during image conversion. To illustrate our approach, we decompose the generator into two parts, the encoder and the decoder, each of which consists of a network of L stages. For any input source domain image x , after passing through L -stage networks of the encoder, a sequence of features of different scales are produced, i.e., $\{h_l\}_1^L = \{G_{enc}^l(h_{l-1})\}_1^L$, where $x = h_0$. Then feeding the output of the last stage of the encoder, i.e., h_L , into the decoder, we can also obtain a sequence of features of different scales in the decoder $\{h_l\}_{L+1}^{2L} = \{G_{dec}^l(h_{l-1})\}_{L+1}^{2L}$, where $\hat{y} = h_{2L}$. Note that h_l and h_{2L-l} are features of the same scale. For brevity, we abbreviate $2L-l$ as \bar{l} in the following and call $(h_l, h_{\bar{l}})$ a pair of same-scale features.

During the forward propagation of the generator, we propose to constrain the semantic consistency of the multi-scale pairwise features of the encoder and decoder, i.e., $\text{similar}(h_l, h_{\bar{l}})$, to ensure the content similarity between the input and generated images, where $\text{similar}(\cdot, \cdot)$ is the content similarity function. We believe this can bring three benefits. First, the optimization distance is shorter: the decoder is directly involved in the computation of the content similarity loss, unlike the CUT-like methods which exert an indirect optimization on the decoder. Second, the training is more efficient because the computation of our content similarity loss is completed in one forward propagation process, and there is no need to re-feed the generated images into the en-

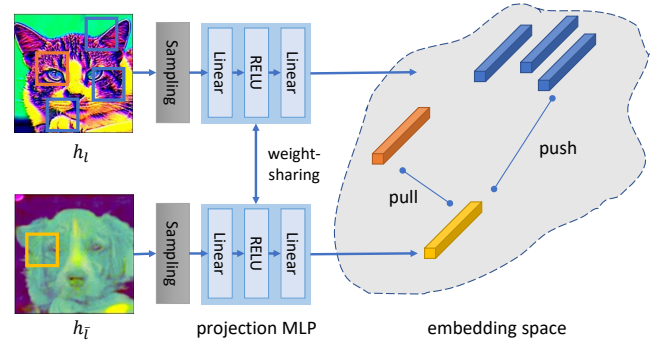


Figure 4: **Pairwise Features Contrastive Loss**. For same-scale feature pairs $(h_l, h_{\bar{l}})$ in the encoder and decoder, we sample query anchor from $h_{\bar{l}}$ and the positive and negatives from h_l according to a specific sampling strategy. We use a weight-sharing projection MLP to cast them into the embedding space, in which we pull the query (yellow) closer to the positive (orange) while pushing it farther away from the negative ones (blue).

coder for secondary encoding. Third, fewer model parameters are required because we do not need an additional encoder to perform the re-encoding. From this point of view, our method can be regarded as an implicit encoding CUT-like approach.

Contrastive Learning-based Semantic Consistency Constraint

Inspired by CUT, we use PatchNCE as the semantic similarity function. Specifically, we apply a noisy contrastive estimation framework to maximize the mutual information between patch-level multi-scale pairwise features between the encoder and decoder to achieve semantic consistency between the input and generated images.

As shown in Figure 4, for any pair of same-scale features $(h_l, h_{\bar{l}})$, we sample a query anchor $q_{\bar{l}}^{(i)}$ from the position (i) of the output feature map of the l -th stage of the decoder $h_{\bar{l}}$ and then sample a positive $k_l^{(i)}$ from the corresponding position (i) of h_l and N negatives $\{k_l^{(j)}\}(i \neq j)$ from the other different positions of h_l . We cast the query anchor, positive, and negatives to the K -dimensional embedding space by only a two-layer projection MLP and obtain vectors $q, k^+ \in \mathbb{R}^K$ and $k^- \in \mathbb{R}^{N \times K}$, respectively. Note that the subscript l is omitted for brevity and v_n^- denotes the representation of the n -th negative in the embedding space.

To avoid collapsing or expanding, we perform L2 normalization on these vectors to map them into the unit sphere. Contrastive learning looks to pull the representation of query and positive closer together in the embedding space, while pushing the representation of query and negatives farther away. This can be built as an $(N+1)$ -way classification problem and is computed using a cross-entropy function that represents the probability of selecting a positive sample from negative ones.

$$l(\mathbf{q}, \mathbf{k}^+, \mathbf{k}^-) = -\log \left[\frac{\exp(\mathbf{q} \cdot \mathbf{k}^+ / \tau)}{\exp(\mathbf{q} \cdot \mathbf{k}^+ / \tau) + \sum_{n=1}^N \exp(\mathbf{q} \cdot \mathbf{k}_n^- / \tau)} \right], \quad (1)$$

where \cdot denotes the vector dot product and τ is the temperature parameter to scale the distance between the query vector and other examples, which we use by default at 0.07.

Further, we can apply this contrastive loss on multi-scale pairwise features $\{(h_l, h_{\bar{l}})\}$, i.e.:

$$\mathcal{L}_{\text{PatchNCE}}(G, H, \mathbf{X}) = \mathbb{E}_{x \sim X} \sum_l^L \sum_s^{\mathbb{S}_l} l(\mathbf{q}_{l,s}, \mathbf{k}_{\bar{l},s}^+, \mathbf{k}_{\bar{l},s}^-), \quad (2)$$

where, \mathbb{L} is the set of chosen same-scale pairwise features to calculate the contrastive loss, and \mathbb{S}_l is the set of sampled query anchors from different positions of $(h_l, h_{\bar{l}})$.

Discriminative Attention-guided Negative Sampling Strategy

In Equation 2, CL-based methods typically adopt a random negative sampling scheme, which may not be efficient enough. In addition, in sampling negatives, previous works might have overlooked the important information from the discriminator: the truthfulness of generated images. We should pay more attention to those regions that the discriminator considered more unrealistic and we should not ignore the regions that the discriminator identifies as true, since the features in these regions are well optimized.

To this end, we propose an efficient discriminative attention-guided (DAG) negative sampling strategy. Assuming that a total of K anchors would be sampled, our proposed negative sample sampling scheme proceeds as follows: 1) obtaining the attention map: for any pair of same-scale features $(h_l, h_{\bar{l}})$, interpolating the output of the discriminator to the same resolution size as h_l and $h_{\bar{l}}$, thus each anchor on h_l receives a attention score; 2) oversampling: uniformly sampling kK ($k > 1$) negatives from h_l ; 3) ranking: sorting in ascending order according to their corresponding attention scores; 4) importance sampling: selecting the top βK important negative samples and the last $(1 - \beta)K$ negative samples.

Full Objective

In addition to the PatchNCE loss presented above, we also use an adversarial loss to complete the domain transfer, and we add an identity mapping loss as a regularization term to stabilize the network training.

Adversarial loss. We use LSGAN loss (Mao et al. 2017) as the adversarial loss to encourage the generated images that are as visually similar to images in the target domain as possible, which is formalized as follows,

$$\mathcal{L}_{\text{GAN}} = \mathbb{E}_{y \sim Y} [D(y)^2] + \mathbb{E}_{x \sim X} [(1 - D(G(x)))^2]. \quad (3)$$

Identity mapping loss. In order to stable the training and accelerate the convergence, we add an identity mapping loss.

$$\mathcal{L}_{\text{identity}}(G) = \mathbb{E}_{y \sim Y} \|G(y) - y\|_1. \quad (4)$$

We only use this regular term in the first half of the training phase because we find that it impacts the generative performance of the network to some extent.

Overall Loss. Our final objective function is as follows:

$$\begin{aligned} \mathcal{L}_{\text{total}}(G, D, H) = & \mathcal{L}_{\text{GAN}}(G, D, X, Y) \\ & + \lambda_{\text{NCE}} \mathcal{L}_{\text{PatchNCE}}(G, H, X) \\ & + \lambda_{\text{IDT}} \mathcal{L}_{\text{identity}}(G), \end{aligned} \quad (5)$$

where λ_{NCE} and λ_{IDT} are set to 2 and 10, respectively.

Experiments

Experiment Setup

Datasets. To demonstrate the superiority of our method, we trained and evaluated on six popular I2I benchmark datasets with eight tasks, including *Cityscapes*, *Cat*↔*Dog*, *Horse*↔*Zebra*, *Label*↔*Facade*, *Winter*↔*Summer* and *Van Gogh*↔*Photo*. *Cityscapes* (Cordts et al. 2016) contains street scenes from German cities with 2975 training images and 500 test images. *Cat*↔*Dog* comes from the AFHQ dataset (Choi et al. 2020), containing 5153 images of cats and 4739 images of dog. *Horse*↔*Zebra*, collected by CycleGAN from ImageNet (Deng et al. 2009), contains 1067 images of horses and 1334 images of zebras. *Winter*↔*Summer* contains 1231 images of summer and 962 images of winter. *Photo*↔*Van Gogh* contains 400 Van Gogh paintings and 6287 photographs from Flickr (Zhu et al. 2017). For all experiments, we resized images to 256 × 256 resolution size.

Implementation details. We use the same ResNet-based generator (Park et al. 2020) and PatchGAN discriminator (Isola et al. 2017) with a receptive field of 70×70. We use Adam optimizer (Kingma and Ba 2014) with $\beta_1 = 0.5$ and $\beta_2 = 0.999$. For the *CityScapes* and *Horse*↔*Zebra* datasets, 400 epoches are trained, and 200 epoches are trained only for the rest of the datasets. Following TTUR (Heusel et al. 2017), we set unbalanced learning rates of $5e - 5$, $2e - 4$ and $5e - 5$ for the generator, discriminator and projection head, respectively. We start linearly decaying the learning rate halfway through the training with batch size of 1.

Evaluation metrics. We mainly use Fréchet Inception Distance (FID) (Heusel et al. 2017) to evaluate the visual quality of the generated images by comparing the distance between distributions of generated and real images in a deep feature domain. We also use improved precision and recall metric (P & R) (Kynkänniemi et al. 2019) as an additional evaluation indicator. Precision indicates the fraction of generated images that looks like the realistic ones, and recall measures the fraction of training data manifold covered by the generator. For the *CityScapes* dataset, since they have corresponding segmentation labels, we apply a pre-trained segmentation model (Yu, Koltun, and Funkhouser 2017) to segment the generated images and use mAP evaluation metric to measure how well methods discover correspondences.

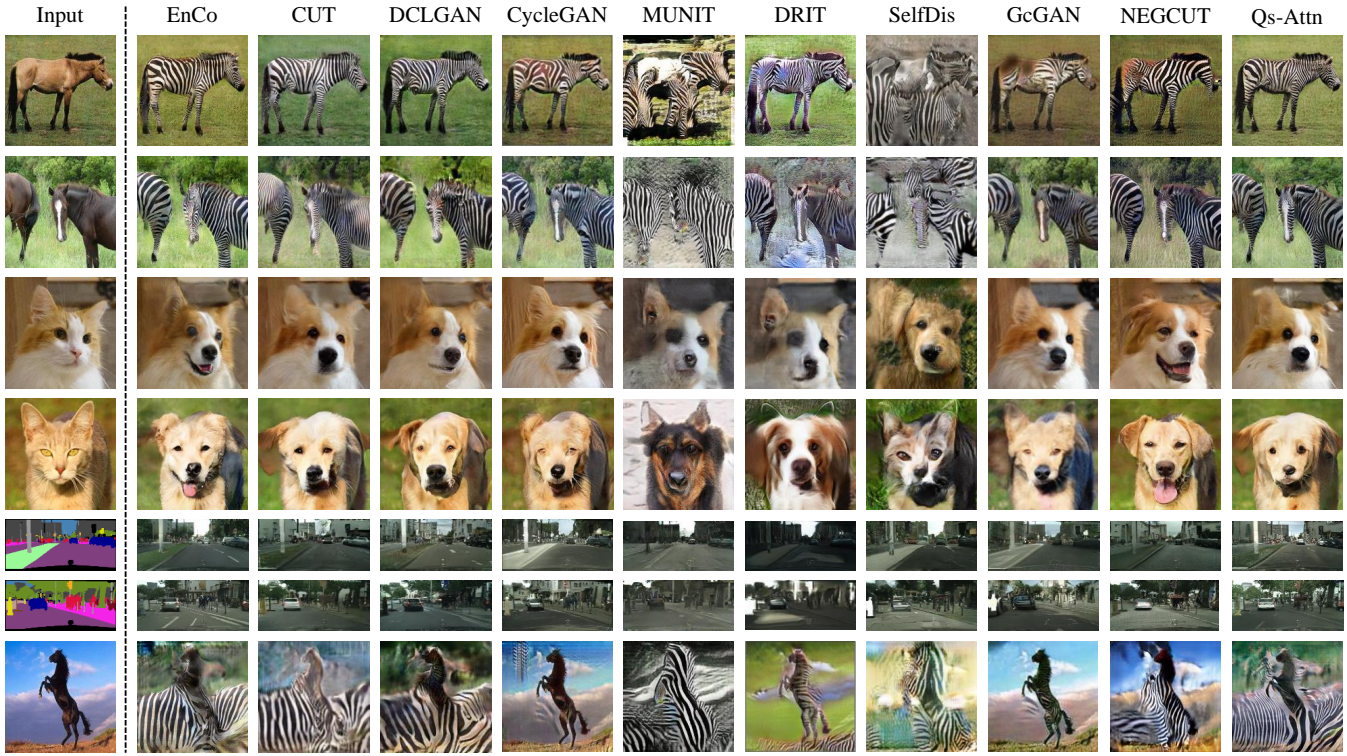


Figure 5: Results of qualitative comparison. We compare EnCo with existing methods on the *Horse*→*Zebra*, *Cat*→*Dog*, and *Cityscapes* datasets. EnCo achieves satisfactory visual results. The final rows show failure cases. Our method are unable to identify the unfamiliar pose of the horse and instead add texture to the background.

Method	CityScapes		Cat→Dog		Horse→Zebra	
	mAP ↑	FID ↓	FID ↓	FID ↓	sec/iter ↓	
CycleGAN	20.4	68.6	85.9	66.8	0.40	
MUNIT	16.9	91.4	104.4	133.8	0.39	
DRIT	17.0	155.3	123.4	140.0	0.70	
DCLGAN	22.9	49.4	60.7	43.2	0.41	
DistanceGAN	8.40	85.8	155.3	72.0	0.15	
SelfDistance	15.3	78.8	144.4	80.8	0.16	
GCGAN	21.2	105.2	96.6	86.7	0.62	
CUT	24.7	56.4	76.2	45.5	0.24	
FSeSim	22.1	54.3	87.8	43.4	0.17	
NEGCUT	25.6	48.5	55.9	40.1	0.57	
QS-Attn	25.8	50.2	80.1	42.8	0.35	
EnCo	23.4	47.6	55.5	39.1	0.14	

Table 1: Comparison with the state-of-the-art methods on unpaired image translation. We show multiple metrics, where the \uparrow indicates higher is better and the \downarrow indicates lower is better. It is worth noting that our method outperforms all baselines on the FID metric and shows competitive results on the *Cityscapes* for the semantic segmentation metric. Also, our method shows a fast training speed.

Comparison with the State-of-the-art Methods

We compare our method with several state-of-the-art methods of unpaired I2I, including CycleGAN (Zhu et al. 2017), MUNIT (Huang et al. 2018), DRIT (Lee et al. 2018), Dis-

tanceGAN, selfDistanceGAN (Benaim and Wolf 2017), GcGAN (Fu et al. 2019), CUT (Park et al. 2020), NEGCUT (Wang et al. 2021), FSeSim (Zheng, Cham, and Cai 2021) and QS-Attn (Hu et al. 2022). Among them, CycleGAN, MUNIT, DRIT and DCLGAN are two-sided methods and the rest are one-sided ones.

The results of the quantitative comparisons are shown in Table 1. As can be seen from Table 1, EnCo outperforms all baselines on FID metric on three datasets. We also achieve a competitive result of mAP metric on the *Cityscapes*. Figure 5 shows the results of the qualitative comparison. Besides, our method exhibits fast training speed with sec/iter 0.14. Compared to DistanceGAN with sec/iter 0.15, we outperforms it by a large margin on FID metric on three datasets. It is worth noting that we need only 23.9% of the training time of the NEGCUT method, which achieves the next best result on FID metric in Table 1.

To further illustrate the advantages of our method over cycle consistency-based and CUT-like methods, we selected CycleGAN, CUT, and DCL on four additional datasets (i.e., *Dog*→*Cat*, *Zebra*→*Horse*, *Winter*→*Summer* and *Van Gogh*→*Photo*) for further comparison. We report additional P & R metric. As shown in Table 2, EnCo still performs superiorly and robustly on various tasks, both on the FID and P & R metric. Our method achieves better performance than DCLGAN on the FID metric, while the parameters are even similar to CUT, and our training time saves 66%, 43.3% and 66.8% compared to CycleGAN, CUT and DCLGAN,

Method	Zebra→Horse		Dog→Cat		Winter→Summer		Photo→Van Gogh			Model Size
	P & R ↑	FID ↓	P & R ↑	FID ↓	P & R ↑	FID ↓	P & R ↑	FID ↓	Training Time ↓	
CycleGAN	43.6 & 53.1	154.3	23.4 & 44.0	103.4	54.2 & 81.5	76.1	16.8 & 11.9	189.0	133.3 hrs	28.286M
CUT	42.3 & 46.4	160.5	62.4 & 57.0	26.8	60.9 & 66.4	86.6	0.9 & 58.6	155.3	80.0 hrs	14.703M
DCLGAN	45.0 & 56.7	139.5	66.2 & 82.4	22.2	63.9 & 72.3	80.3	13.5 & 32.2	149.5	136.7 hrs	29.274M
EnCo	47.9 & 47.1	146.8	65.4 & 84.2	22.1	60.1 & 82.4	71.6	30.0 & 48.1	125.1	45.3 hrs	14.456M

Table 2: **Comparison with CycleGAN, CUT, and DCLGAN alone.** We conducted a further comparison with cycle consistency-based methods and CUT-like methods on four other tasks, i.e., *Zebra→Horse*, *Dog→Cat*, *Winter→Summer* and *Photo→Van Gogh*. EnCo still outperforms both the cycle consistency-based and CUT-like methods in most tasks. We also report the overall runtimes for *Photo→Van Gogh* task and the metric of model parameters for all tasks.

Configurations	Training settings			Cat→Dog		Horse→Zebra			sec/iter ↓
	MS	DAG	SP	P & R ↑	FID ↓	P & R ↑	FID ↓	sec/iter ↓	
A $(h_7, h_{24}\#128)$	✗	✓	✓	45.6 & 70.0	67.6	50.8 & 65.0	46.8	0.129	
B $(h_3, h_{28}\#256), (h_7, h_{24}\#128)$	✓	✓	✓	65.4 & 72.8	64.6	53.3 & 75.0	45.7	0.134	
C $(h_7, h_{24}\#128), (h_{13}, h_{18}\#64)$	✓	✓	✓	68.2 & 74.0	62.5	53.3 & 69.7	42.6	0.134	
D uniform sampling	✓	✗	✓	73.4 & 71.4	63.8	60.2 & 72.5	43.1	0.133	
E two projectors	✓	✓	✗	67.2 & 69.0	66.0	60.0 & 73.3	46.9	0.136	
F default	✓	✓	✓	72.6 & 78.6	55.5	63.3 & 72.8	39.1	0.136	

Table 3: **Quantitative results for ablations.** MS: multi-scale pairwise features. DAG: discriminative attention-guided negative sampling strategy. SP: shared projection MLP.

respectively, on the *Photo→Van Gogh* task.

Ablation Study

Compared to baselines, our method exhibits superior performance. We design several ablation experiments to analyze each contribution of components in isolation. We mainly conduct ablation experiments on three datasets, *Cat→Dog*, *Label→Facade*, *Horse→Zebra*. We report the results of ablation experiments in Table 3.

Constraints on multi-scale pairwise features are important. EnCo selects three pairs of same-scale features (h_3, h_{28}) , (h_7, h_{24}) , and (h_{13}, h_{18}) in default, whose corresponding feature maps are at resolutions size of 256×256 , 128×128 , and 64×64 , respectively. More architecture details refer to Appendix.D. From row A-C in Table 3, we can observe that the model performance gains in different degrees as we add more pairs of same-scale features with different semantic levels.

The DAG negative sampling strategy significantly boost the model performance. We also conducted the ablation experiments for the negative sampling strategy. As can be seen from row D in Table 3, when we remove the DAG negative sampling strategy, i.e., use the random strategy, the performance of the model on each task shows different degrees of degradation, which fully demonstrates the effectiveness of DAG negative sampling strategy.

Weight-sharing projection MLP is more efficient than two. DCLGAN claims that two independent projection MLPs help to distinguish the gap between the two domains. However, in our experiments (see row E in the Table 3), it

was found that two projection MLPs did not work as well as when their network weights were shared, that is, only one projection MLP available. We believe that this is because the semantic level of the same scale features is about the same, so only one projection MLP is sufficient to accomplish the embedding. In addition, receiving feature information from both the encoder and decoder helps the projection MLP to distinguish between the two domains.

Conclusion

In this paper, we propose a novel framework EnCo for one-sided image translation. EnCo preserves content by explicitly constraining the semantic consistency of multi-scale pairwise features between the encoder and decoder of generator. By rethinking the role of the discriminator in sampling negatives, we propose a discriminative attention-based negative sampling strategy with almost negligible computational overhead that boosts the generative model performance significantly. Compared to others, our approach is more flexible and efficient as the content consistency is constrained in one forward propagation without extra re-encoding or re-feeding images to map them into a predefined distance space. Extensive experiments on several benchmark datasets have demonstrated the efficiency and effectiveness of EnCo. We hope EnCo will bring some new thoughts and inspiration to the paradigm of contrastive learning applied to I2I tasks.

References

Benaim, S.; and Wolf, L. 2017. One-sided unsupervised domain mapping. In *Advances in neural information processing systems (NIPS)*, 752–762.

Cai, T. T.; Frankle, J.; Schwab, D. J.; and Morcos, A. S. 2020. Are all negatives created equal in contrastive instance discrimination? *arXiv preprint arXiv:2010.06682*.

Chen, R.; Huang, W.; Huang, B.; Sun, F.; and Fang, B. 2020a. Reusing discriminators for encoding: Towards unsupervised image-to-image translation. In *Proceedings of the IEEE/CVF conference on computer vision and pattern recognition*, 8168–8177.

Chen, T.; Kornblith, S.; Norouzi, M.; and Hinton, G. 2020b. A simple framework for contrastive learning of visual representations. In *International Conference on Machine Learning (ICML)*.

Choi, Y.; Uh, Y.; Yoo, J.; and Ha, J.-W. 2020. Stargan v2: Diverse image synthesis for multiple domains. In *Proceedings of the IEEE/CVF conference on computer vision and pattern recognition*, 8188–8197.

Chopra, S.; Hadsell, R.; and LeCun, Y. 2005. Learning a similarity metric discriminatively, with application to face verification. In *2005 IEEE Computer Society Conference on Computer Vision and Pattern Recognition (CVPR'05)*, volume 1, 539–546. IEEE.

Cordts, M.; Omran, M.; Ramos, S.; Rehfeld, T.; Enzweiler, M.; Benenson, R.; Franke, U.; Roth, S.; and Schiele, B. 2016. The cityscapes dataset for semantic urban scene understanding.

Deng, J.; Dong, W.; Socher, R.; Li, L.-J.; Li, K.; and Fei-Fei, L. 2009. Imagenet: A large-scale hierarchical image database. In *IEEE conference on computer vision and pattern recognition (CVPR)*, 248–255. Ieee.

Dong, Y.; Liu, Y.; Zhang, H.; Chen, S.; and Qiao, Y. 2020. FD-GAN: Generative adversarial networks with fusion-discriminator for single image dehazing. In *Proceedings of the AAAI Conference on Artificial Intelligence*, volume 34, 10729–10736.

Fu, H.; Gong, M.; Wang, C.; Batmanghelich, K.; Zhang, K.; and Tao, D. 2019. Geometry-consistent generative adversarial networks for one-sided unsupervised domain mapping. In *IEEE Conference on Computer Vision and Pattern Recognition (CVPR)*, 2427–2436.

Goodfellow, I.; Pouget-Abadie, J.; Mirza, M.; Xu, B.; Warde-Farley, D.; Ozair, S.; Courville, A.; and Bengio, Y. 2014. Generative adversarial nets. *Advances in neural information processing systems*, 27.

Han, J.; Shoeiby, M.; Petersson, L.; and Armin, M. A. 2021. Dual contrastive learning for unsupervised image-to-image translation. In *Proceedings of the IEEE/CVF Conference on Computer Vision and Pattern Recognition*, 746–755.

He, K.; Fan, H.; Wu, Y.; Xie, S.; and Girshick, R. 2020. Momentum contrast for unsupervised visual representation learning. In *IEEE Conference on Computer Vision and Pattern Recognition (CVPR)*, 9729–9738.

Henaff, O. 2020. Data-efficient image recognition with contrastive predictive coding. In *ICML*, 4182–4192. PMLR.

Heusel, M.; Ramsauer, H.; Unterthiner, T.; Nessler, B.; and Hochreiter, S. 2017. Gans trained by a two time-scale update rule converge to a local nash equilibrium. *Advances in neural information processing systems*, 30.

Hjelm, R. D.; Fedorov, A.; Lavoie-Marchildon, S.; Grewal, K.; Bachman, P.; Trischler, A.; and Bengio, Y. 2018. Learning deep representations by mutual information estimation and maximization. *arXiv preprint arXiv:1808.06670*.

Hu, Q.; Wang, X.; Hu, W.; and Qi, G.-J. 2021. Adco: Adversarial contrast for efficient learning of unsupervised representations from self-trained negative adversaries. In *Proceedings of the IEEE/CVF Conference on Computer Vision and Pattern Recognition*, 1074–1083.

Hu, X.; Zhou, X.; Huang, Q.; Shi, Z.; Sun, L.; and Li, Q. 2022. QS-Attn: Query-Selected Attention for Contrastive Learning in I2I Translation. In *Proceedings of the IEEE/CVF Conference on Computer Vision and Pattern Recognition*, 18291–18300.

Huang, X.; Liu, M.-Y.; Belongie, S.; and Kautz, J. 2018. Multimodal unsupervised image-to-image translation. In *European Conference on Computer Vision (ECCV)*, 172–189.

Isola, P.; Zhu, J.-Y.; Zhou, T.; and Efros, A. A. 2017. Image-to-Image Translation with Conditional Adversarial Networks. In *IEEE Conference on Computer Vision and Pattern Recognition (CVPR)*.

Kim, T.; Cha, M.; Kim, H.; Lee, J. K.; and Kim, J. 2017. Learning to discover cross-domain relations with generative adversarial networks. In *International Conference on Machine Learning (ICML)*.

Kingma, D. P.; and Ba, J. 2014. Adam: A method for stochastic optimization. *International Conference on Learning Representations (ICLR)*.

Kirillov, A.; Wu, Y.; He, K.; and Girshick, R. 2020. Pointrend: Image segmentation as rendering. In *Proceedings of the IEEE/CVF conference on computer vision and pattern recognition*, 9799–9808.

Kynkänniemi, T.; Karras, T.; Laine, S.; Lehtinen, J.; and Aila, T. 2019. Improved precision and recall metric for assessing generative models. *Advances in Neural Information Processing Systems*, 32.

Lee, H.-Y.; Tseng, H.-Y.; Huang, J.-B.; Singh, M.; and Yang, M.-H. 2018. Diverse image-to-image translation via disentangled representations. In *European conference on computer vision (ECCV)*, 35–51.

Liang, J.; Cao, J.; Sun, G.; Zhang, K.; Van Gool, L.; and Timofte, R. 2021. Swinir: Image restoration using swin transformer. In *Proceedings of the IEEE/CVF International Conference on Computer Vision*, 1833–1844.

Lin, Y.; Zhang, S.; Chen, T.; Lu, Y.; Li, G.; and Shi, Y. 2022. Exploring Negatives in Contrastive Learning for Unpaired Image-to-Image Translation. *arXiv preprint arXiv:2204.11018*.

Liu, M.-Y.; Breuel, T.; and Kautz, J. 2017. Unsupervised image-to-image translation networks. In *Advances in neural information processing systems (NIPS)*, 700–708.

Mao, X.; Li, Q.; Xie, H.; Lau, R. Y.; Wang, Z.; and Paul Smolley, S. 2017. Least squares generative adversarial networks. In *Proceedings of the IEEE international conference on computer vision*, 2794–2802.

Oord, A. v. d.; Li, Y.; and Vinyals, O. 2018. Representation learning with contrastive predictive coding. *arXiv preprint arXiv:1807.03748*.

Park, T.; Efros, A. A.; Zhang, R.; and Zhu, J.-Y. 2020. Contrastive Learning for Unpaired Image-to-Image Translation. In *European Conference on Computer Vision (ECCV)*.

Qian, R.; Meng, T.; Gong, B.; Yang, M.-H.; Wang, H.; Belongie, S.; and Cui, Y. 2021. Spatiotemporal contrastive video representation learning. In *Proceedings of the IEEE/CVF Conference on Computer Vision and Pattern Recognition*, 6964–6974.

Rao, J.; He, H.; and Lin, J. 2016. Noise-contrastive estimation for answer selection with deep neural networks. In *Proceedings of the 25th ACM International Conference on Information and Knowledge Management*, 1913–1916.

Robinson, J.; Chuang, C.-Y.; Sra, S.; and Jegelka, S. 2020. Contrastive learning with hard negative samples. *arXiv preprint arXiv:2010.04592*.

Shrivastava, A.; Pfister, T.; Tuzel, O.; Susskind, J.; Wang, W.; and Webb, R. 2017. Learning from simulated and unsupervised images through adversarial training. In *Proceedings of the IEEE conference on computer vision and pattern recognition*, 2107–2116.

Simonyan, K., and Zisserman, A. 2015. Very deep convolutional networks for large-scale image recognition.

Ulyanov, D.; Vedaldi, A.; and Lempitsky, V. 2016. Instance normalization: The missing ingredient for fast stylization. *arXiv preprint arXiv:1607.08022*.

Wang, J.; Yu, L.; Zhang, W.; Gong, Y.; Xu, Y.; Wang, B.; Zhang, P.; and Zhang, D. 2018a. A minimax game for unifying generative and discriminative information retrieval models. *SIGIR Proc.*

Wang, T.-C.; Liu, M.-Y.; Zhu, J.-Y.; Tao, A.; Kautz, J.; and Catanzaro, B. 2018b. High-Resolution Image Synthesis and Semantic Manipulation with Conditional GANs. In *IEEE Conference on Computer Vision and Pattern Recognition (CVPR)*.

Wang, W.; Zhou, W.; Bao, J.; Chen, D.; and Li, H. 2021. Instance-wise hard negative example generation for contrastive learning in unpaired image-to-image translation. In *Proceedings of the IEEE/CVF International Conference on Computer Vision*, 14020–14029.

Yi, Z.; Zhang, H.; Tan, P.; and Gong, M. 2017. Dualgan: Unsupervised dual learning for image-to-image translation. In *IEEE International Conference on Computer Vision (ICCV)*, 2849–2857.

Ying, R.; He, R.; Chen, K.; Eksombatchai, P.; Hamilton, W. L.; and Leskovec, J. 2018. Graph convolutional neural networks for web-scale recommender systems. In *Proceedings of the 24th ACM SIGKDD international conference on knowledge discovery & data mining*, 974–983.

Yu, F.; Koltun, V.; and Funkhouser, T. 2017. Dilated residual networks. In *IEEE conference on computer vision and pattern recognition (CVPR)*, 472–480.

Yuan, Y.; Liu, S.; Zhang, J.; Zhang, Y.; Dong, C.; and Lin, L. 2018. Unsupervised image super-resolution using cycle-in-cycle generative adversarial networks. In *IEEE Conference on Computer Vision and Pattern Recognition Workshops (CVPRW)*, 701–710.

Zhang, R.; Isola, P.; and Efros, A. A. 2016. Colorful image colorization. In *European conference on computer vision (ECCV)*, 649–666. Springer.

Zhang, W.; Chen, T.; Wang, J.; and Yu, Y. 2013. Optimizing top-n collaborative filtering via dynamic negative item sampling. In *Proceedings of the 36th international ACM SIGIR conference on Research and development in information retrieval*, 785–788.

Zheng, C.; Cham, T.-J.; and Cai, J. 2021. The spatially-correlative loss for various image translation tasks. In *Proceedings of the IEEE/CVF Conference on Computer Vision and Pattern Recognition*, 16407–16417.

Zhu, J.-Y.; Park, T.; Isola, P.; and Efros, A. A. 2017. Unpaired Image-to-Image Translation using Cycle-Consistent Adversarial Networks. In *IEEE International Conference on Computer Vision (ICCV)*.

Appendix

A. Limitations

We focus here on the limitations of our method and the experiments part. An important ingredient of our proposed approach is the choice of same-scale pairwise features, which has a crucial effect on the optimization of EnCo. We mainly use the ResNet-like generator following CUT (refer to Table 5 for more model details) and we mainly select 3 same-scale feature pairs, $(h_3, h_{28}, \#256)$, $(h_7, h_{24}, \#128)$ and $(h_{13}, h_{18}, \#64)$, where the number after $\#$ represents the resolution size of the features. We do not explore the choice of more same-scale feature pairs, such as $(h_{12}, h_{29}, \#64)$, because of limited computational resources. What is more, our proposed discriminative attention-guided (DAG) negative sampling strategy is flexible and can be applied to other CL-based methods, such as CUT and its bidirectional version DCLGAN. However, we did not conduct this part of experiments due to limited training resources also. We potentially believe that our proposed DAG negative sample strategy can have a positive impact on the optimization process of these methods.

B. Discriminative Attention-guided Negative Sampling Algorithm

We provide the pseudo-code of the DAG negative sampling strategy in PyTorch style in Algorithm 1.

C. More Generated Results

We show additional comparison results for *Cityscapes*, *Horse*→*Zebra* and *Cat*→*Dog* tasks in Figure 8, Figure 9 and Figure 10, respectively. This is an extension of Figure 5 in the main paper. We only show the results of CycleGAN, CUT, DCLGAN, NEGCUT and QS-Attn in these figures. They achieved challenging results in Table 1.

D. Architecture of Networks

Following CycleGAN and CUT, We use a ResNet-like generator. The detailed generator architecture is shown in Table 5. Conv2d uses kernel size 3, padding 1 and stride 1 except for the first Conv2d using a large kernel size 7, padding 3 and stride 1. IN means instance normalization. Resnet-Block consists of Conv2d, IN, ReLU, Conv2d and IN. We decompose the generator G into two parts, the encoder and decoder. CUT assigns the first 5 ResnetBlocks to the encoder while we assign the 5-th ResnetBlock to the decoder for symmetry reason. We also apply a PatchGAN discriminator as CycleGAN and Pix2Pix. As shown in Table 6, the discriminator in our model contains three down-sampling blocks and outputs a 30×30 feature map, each element in which correspond to a 70×70 patch in the input image.

E. More Ablations

Our proposed DGA negative sampling strategy significantly boost the generative performance of model performance. We also conducted additional ablation experiments on the oversampling rate and the importance sampling rate (as shown in Table 4). We find that a large importance sampling rate is

Algorithm 1: DAG Pseudocode, PyTorch-like

```

1   # H: height, W: width, C: dimension
2   # K: number of negatives to sample
3   # k: oversampling ratio
4   # beta: importance sampling ratio
5   # feat: input tensor (H, W, C)
6   # score_map: spatial attention tensor, (H, W)
7
8   H, W, C = feat.shape
9   feat_reshape = feat.flatten(0, 1)
10  # oversampling
11  points_os = torch.randperm(H * W) [:k * K]
12  scores_os = score_map.flatten() [points_os]
13  # sorting
14  _, indices = torch.sort(scores_os, descending=
15  # importance sampling
16  idx_high = points_os[indices[:beta * K]]
17  idx_low = points_os[indices[(beta - 1) * K:]]
18  idx_sampled = torch.cat([idx_high, idx_low])
19
20  feat_to_return = feat_reshape[idx_sampled, :]

```

not friendly to the I2I tasks, which may be a result of over-focusing on hard sample regions and thus the instability of training. Also through experiments, we find that the optimized margin yields better performance when the oversampling rate is set to 4.

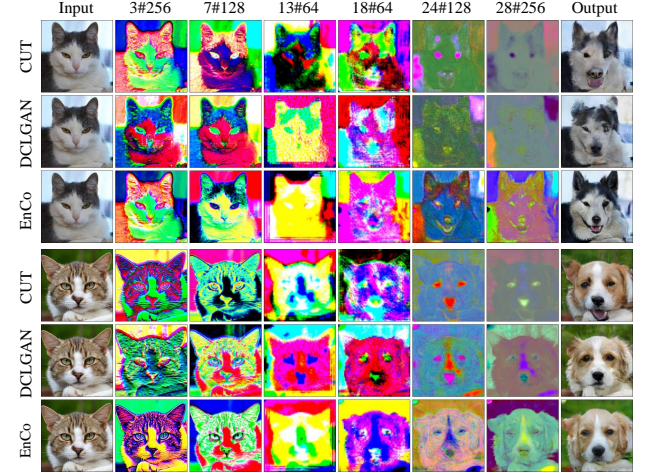


Figure 6: **Visualization of multi-scale pairwise features the of encoder and decoder of the generator.** we visualize the top 3 PCA components of multi-scale pairwise features in the generator, i.e., $(h_3, h_{28}, \#256)$, $(h_7, h_{24}, \#128)$ and $(h_{13}, h_{18}, \#64)$, where $\#x$ indicates the resolution size of features.

F. Visualization of Multi-scale Pairwise Features

To further analyze the role of constraints of multi-scale pairwise features in the image transformation process, we visualized the selected pairs of features. Specifically, we performed PCA dimensionality reduction on the output features of the 3, 7, 13, 18, 24, 28-th layers of the network, respectively, and the visualization results are shown in Figure 6.

Method	Cat→Dog		Horse→Zebra
	FID ↓	FID ↓	sec/iter
uniform ($k = 1, \beta = 0.0$)	63.8	43.1	0.133
midly biased ($k = 4, \beta = 0.75$)	65.9	50.6	0.134
heavily biased ($k = 4, \beta = 1.0$)	70.8	47.6	0.134
small margin ($k = 2, \beta = 0.5$)	62.4	42.3	0.134
large margin ($k = 8, \beta = 0.5$)	64.8	44.0	0.135
default ($k = 4, \beta = 0.5$)	55.5	39.1	0.134

Table 4: **Ablations on oversampling ratio k and importance sampling ratio β of DAG negative sampling strategy.**

We can first see that under the semantic consistency constraint of the multi-scale pairwise features, the feature maps of the decoder network of the generator in our method contain richer details than those of the implicitly constrained decoder methods such as CUT and DCLGAN. This potentially indicates that our method has a more proactive effect on the decoder. Also, we can see that the semantic levels between same-scale features are similar and different same-scale feature pairs focus on different semantic levels, e.g., (h_4, h_{25}) contains more texture-like information, while (h_{12}, h_{17}) has more color blocks, indicating that it is more likely to focus on the relationship between parts, which may explain why the semantic consistency constraint for multi-scale pairwise features performs better.

G. Evaluation Details

We list the details of our evaluation protocol.

Fréchet Inception Distance (FID (Heusel et al. 2017)) is computed by measuring the mean and variance distance of the generated and real images in a deep feature space. We first resize the images to 299×299 , and then feed them into a pretrained Inception model to extract deep features. Here, we used the default setting of <https://github.com/mseitzer/pytorch-fid> to compute the FID score on test set images.

For mAP, the semantic segmentation metrics on the *Cityscapes* dataset, we used a pretrained DRN-D-22 model to segment the generated images and compared with the corresponding ground truth labels. Specifically, the pretrained DRN-D-22 model are provided in <https://github.com/WeilunWang/NEGCUT>, which was trained with batch size 32 and learning rate 0.01, for 250 epochs at 256x128 resolution and the original training code is provided in <https://github.com/fyu/drn>. Before passed to the segmentation model, we resized the input images to 256x128 using bicubic downsampling and the ground truth labels were downsampled to the same size using nearest-neighbor sampling.

For the improved precision and recall metric (P & R), we used an Inception pretrained model to embed images into a high-dimensional manifold space. Precision is quantified by querying for each generated image whether the image is within the estimated manifold of real images. Symmetrically, recall is calculated by querying for each real image whether the image is within estimated manifold of gen-

erated images. We thank <https://github.com/photosynthesis-team/piq> for providing the evaluation interface for P & R.

Encoder			Decoder		
Name	Operations	Output Size	Name	Operations	Output Size
h_0	Input	$256 \times 256 \times 3$	h_{31}	Conv2d,Tanh,Output	$256 \times 256 \times 3$
h_3	Conv2d,IN,ReLU	$256 \times 256 \times 64$	h_{28}	Conv2d,IN,ReLU	$256 \times 256 \times 64$
h_6	Conv2d,IN,ReLU	$256 \times 256 \times 128$	h_{25}	Upsample	$256 \times 256 \times 128$
h_7	Downsample	$128 \times 128 \times 128$	h_{24}	Conv2d,IN,ReLU	$128 \times 128 \times 128$
h_{10}	Conv2d,IN,ReLU	$128 \times 128 \times 256$	h_{21}	Upsample	$128 \times 128 \times 256$
h_{11}	Downsample	$64 \times 64 \times 256$	h_{20}	ResnetBlock	$64 \times 64 \times 256$
h_{12}	ResnetBlock	$64 \times 64 \times 256$	h_{19}	ResnetBlock	$64 \times 64 \times 256$
h_{13}	ResnetBlock	$64 \times 64 \times 256$	h_{18}	ResnetBlock	$64 \times 64 \times 256$
h_{14}	ResnetBlock	$64 \times 64 \times 256$	h_{17}	ResnetBlock	$64 \times 64 \times 256$
h_{15}	ResnetBlock	$64 \times 64 \times 256$	h_{16}	ResnetBlock	$64 \times 64 \times 256$

Table 5: **Architecture of the generator.**

Name	Operations	Output Size
h_0	Input	$256 \times 256 \times 3$
h_3	Conv2d,LeakyReLU	$255 \times 255 \times 64$
h_7	Downsample	$128 \times 128 \times 64$
h_6	Conv2d,IN,LeakyReLU	$127 \times 127 \times 128$
h_7	Downsample	$64 \times 64 \times 128$
h_{10}	Conv2d,IN,LeakyReLU	$63 \times 63 \times 256$
h_{11}	Downsample	$32 \times 32 \times 256$
h_{10}	Conv2d,IN,LeakyReLU	$31 \times 31 \times 256$
h_{12}	Conv2d	$30 \times 30 \times 1$

Table 6: **Architecture of the discriminator.**

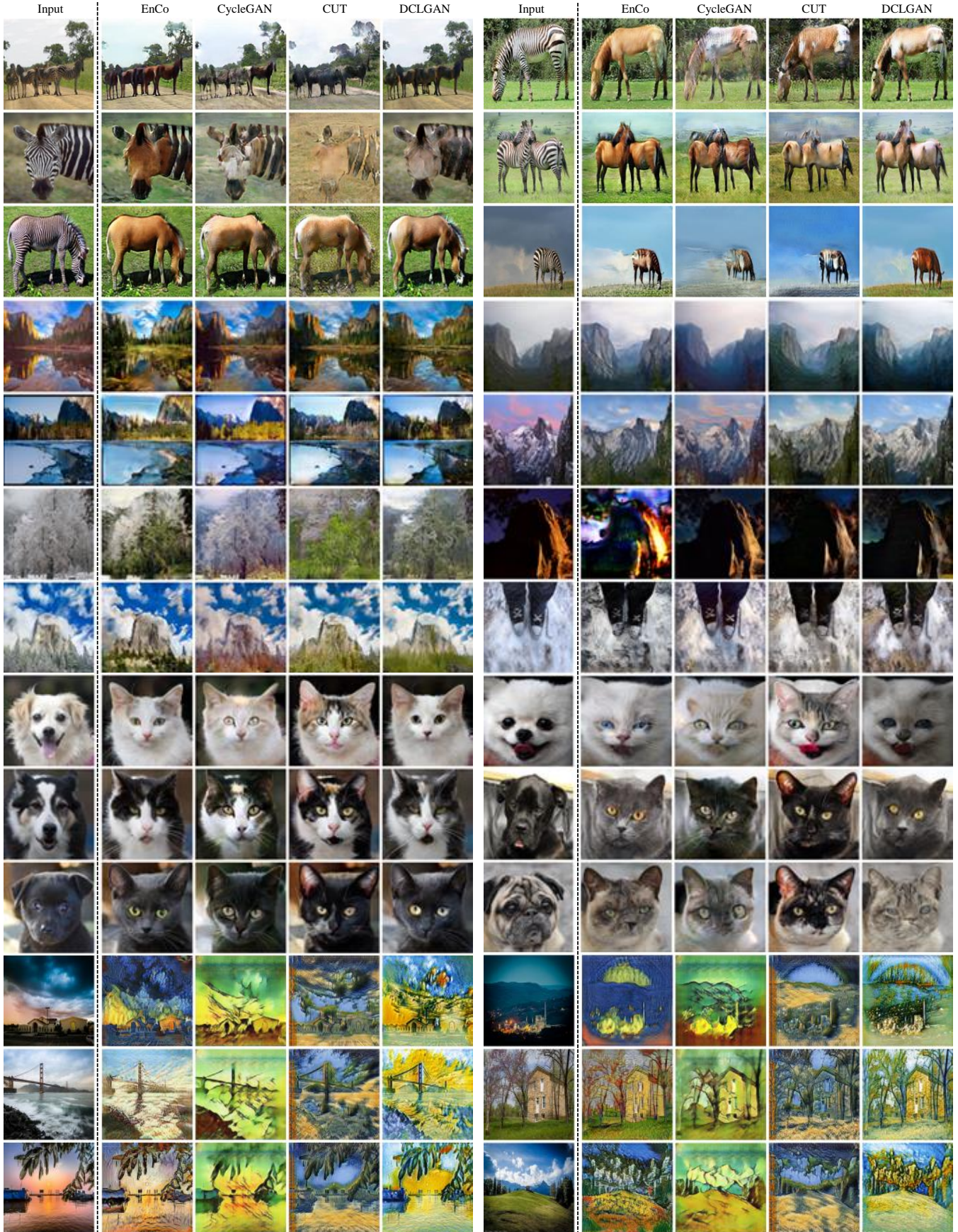


Figure 7: **Qualitative results.** From top to bottom, we show the visual comparison on the *Zebra*→*Horse*, *Winter*→*Summer*, *Dog*→*Cat* and *Photo*→*Van Gogh*.





Figure 9: More results of qualitative comparison on the *Horse→Zebra* dataset.

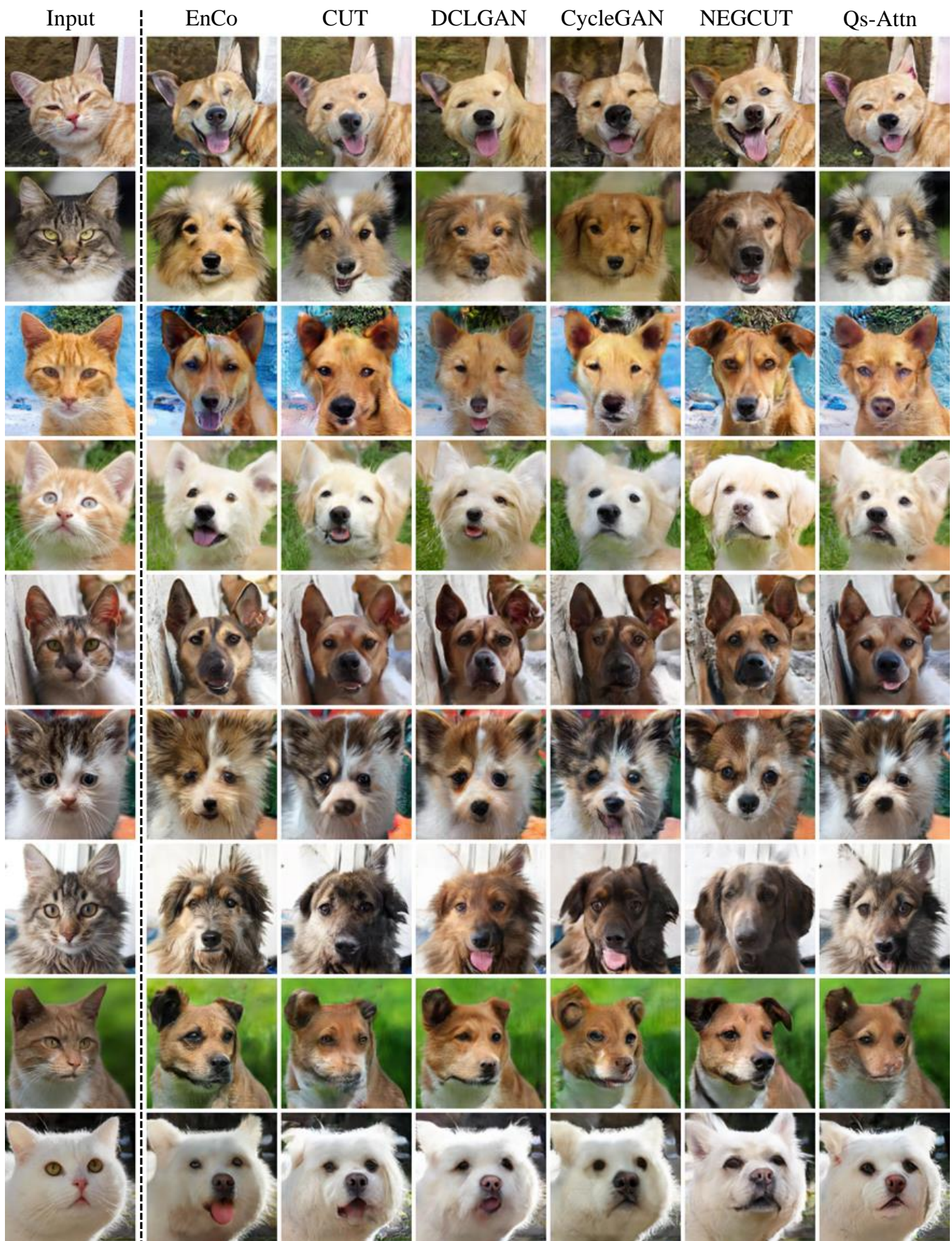


Figure 10: More results of qualitative comparison on the *Cat*→*Dog* dataset.